Phase aberration correction by correlation in digital holographic adaptive optics

Changgeng Liu, Xiao Yu, and Myung K. Kim*

Digital Holography and Microscopy Laboratory, Department of Physics University of South Florida, Tampa, Florida 33620, USA

*Corresponding author: mkkim@usf.edu

Received 25 January 2013; revised 27 March 2013; accepted 27 March 2013;
posted 27 March 2013 (Doc. ID 184105); published 19 April 2013

We present a phase aberration correction method based on the correlation between the complex full-field and guide-star holograms in the context of digital holographic adaptive optics (DHAO). Removal of a global quadratic phase term before the correlation operation plays an important role in the correction. Correlation operation can remove the phase aberration at the entrance pupil plane and automatically refocus the corrected optical field. Except for the assumption that most aberrations lie at or close to the entrance pupil, the presented method does not impose any other constraints on the optical systems. Thus, it greatly enhances the flexibility of the optical design for DHAO systems in vision science and microscopy. Theoretical studies show that the previously proposed Fourier transform DHAO (FTDHAO) is just a special case of this general correction method, where the global quadratic phase term and a defocus term disappear. Hence, this correction method realizes the generalization of FTDHAO into arbitrary DHAO systems. The effectiveness and robustness of this method are demonstrated by simulations and experiments.

OCIS codes: (090.1995) Digital holography; (010.1080) Active or adaptive optics; (170.4460) Ophthalmic optics and devices; (170.0180) Microscopy.

http://dx.doi.org/10.1364/AO.52.002940

1. Introduction

Adaptive optics (AO) was initially presented to eliminate or alleviate the image distortion due to the atmospheric turbulence in astronomy [1]. Nowadays, AO has become necessary for most of major ground-based telescopes [2,3]. Similar to the ground-based telescopes, the human eye also suffers from many monochromatic aberrations. In 1994, the Shack–Hartmann wavefront sensor used in astronomy was first adopted to measure the ocular aberrations of the human eyes by Bille's group [4]. The first AO system for vision science was assembled by Liang *et al.* in 1997 [5]. Using this system, the retinal images at the cellular scale were obtained. Since that time, AO in vision science has seen rapid growth with more and more systems being developed [6–11]. AO has also demonstrated success in microscopy [12]. The aberrations induced by variations of refractive index through the sample can be reduced through the AO system [13]. A typical AO system includes several critical hardware pieces: deformable mirror, lenslet array, and a second CCD camera in addition to the camera for imaging. A novel AO system was recently proposed to replace these hardware components with numerical processing for wavefront measurement and compensation of aberration through the principles of digital holography [14–19].

In the original digital holographic adaptive optics (DHAO) system, the CCD was put in the image plane of the pupil [14]. Although we can obtain a direct measurement of the wavefront at the pupil, the imaging lens other than the eye lens will introduce spherical curvature that has to be removed by additional matching lens in the reference beam. Also, the correct guide-star hologram is difficult to obtain. To get a focused image, numerical propagation is necessary.

1559-128X/13/122940-10$15.00/0

To address these issues, Fourier transform DHAO (FTDHAO) system was proposed [20]. The CCD was put at the Fourier transform (FT) plane of the pupil, instead of the image plane. No spherical curvature was induced by the imaging lens. The CCD could directly record the point spread function (PSF) of the system, facilitating the determination of the correct guide-star hologram. In addition, with some modifications, low coherence or even incoherent light source may be incorporated [21–26]. Notwithstanding these advantages over the original DHAO, the correction method in FTDHAO has significant constraint in the optical configuration. In this paper, we present a more general and flexible correction method. FTDHAO becomes a special case of this generalized method. It is realized through the correlation between the complex full-field hologram and the guide-star hologram after removal of a global quadratic phase term. This correlation operation can eliminate both the aberration at the entrance pupil and the defocus term, obtaining a corrected and focused image, no matter where the CCD is placed. Except for the assumption that the optical aberrations mainly lie at or close to the pupil plane, the correlation method does not set any other requirement on the optical system. Therefore, it will greatly improve the flexibility of the optical design for AO in vision science and microscopy. The correlation method cannot only maintain the merits possessed by FTDHAO, but also can be applied for any DHAO systems. It is worth noting that a similar method was used in incoherent DHAO [23,24]. However, in principle, it is different from the method presented in this paper. Correlation operation used in incoherent DHAO results in corrected intensity instead of corrected complex amplitude. The observations on the global phase term and the defocus term presented in this paper were not shown in the method for incoherent DHAO [23,24].

Section 2 presents a detailed mathematical description of this correction method. In this section, the sampling requirements are also discussed. In Section 3, three simulation examples are given. Corresponding to the simulations, the experiments are described and discussed in Section 4. The major conclusions are summarized in Section 5.

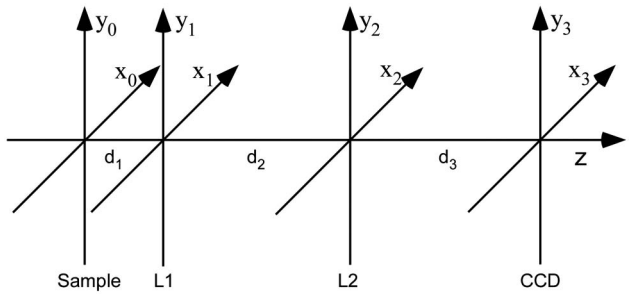

Fig. 1. Coordinates for a two-lens optical system.

2. Principles

A typical DHAO process includes phase aberration measurement, full-field imaging, and image correction. The phase aberration is retrieved from a guide-star hologram while the full-field image is obtained from a full-field hologram that is distorted by the aberration. The image is recovered by removing the measured phase aberration from the distorted full-field image [14,20]. In this paper, we treat the correction from a different point of view by taking correlation of the complex full-field hologram with the complex guide-star hologram. Although the derivation is based on a two-lens system, the generalization of the conclusion to arbitrary optical systems is straightforward. The coordinates adopted for this two-lens system are illustrated in Fig. 1. For the purpose of brevity, one dimension is adopted in the derivation. Assume the pupil of the lens L1 is the entrance pupil of the system. The aberration-free pupil function is represented by $P(x_1)$, and the phase aberration at the pupil is denoted by $\Phi(x_1)$. The focal lengths of the lens L1 and L2 are f_1 and f_2, respectively. Distances d_1, d_2, and d_3 are as defined in Fig. 1. The amplitude PSF of this system is given by

$$
\begin{aligned}
G(x_3,x_0) &= \int_{-\infty}^{+\infty} \mathrm{d}x_2 \exp\left[\frac{j\pi}{\lambda d_3}(x_3-x_2)^2\right] \exp\left(-\frac{j\pi}{\lambda f_2}x_2^2\right)\left\{\exp\left(\frac{j\pi}{\lambda d_2}x_2^2\right)\int_{-\infty}^{+\infty}\mathrm{d}x_1 A(x_0)\right.\\
&\quad\left.\times \exp\left[\frac{j\pi}{\lambda d_1}(x_1-x_0)^2\right]P(x_1)\Phi(x_1)\exp\left(-\frac{j\pi}{\lambda f_1}x_1^2\right)\exp\left(\frac{j\pi}{\lambda d_2}x_1^2\right)\exp\left(\frac{-j2\pi}{\lambda d_2}x_1x_2\right)\right\}\\
&= \exp\left(\frac{j\pi}{\lambda d_3}x_3^2\right)\exp\left(\frac{j\pi}{\lambda d_1}x_0^2\right)A(x_0)\int_{-\infty}^{+\infty}\mathrm{d}x_1 P(x_1)\Phi(x_1)\exp\left[\frac{j\pi}{\lambda}\left(\frac{1}{d_1}+\frac{1}{d_2}-\frac{1}{f_1}\right)x_1^2\right]\exp\left(\frac{-j2\pi}{\lambda d_1}x_0x_1\right)\\
&\quad\times\left[\int_{-\infty}^{+\infty}\mathrm{d}x_2\exp\left(\frac{j\pi}{\lambda d_2}x_2^2\right)\exp\left(\frac{j\pi}{\lambda d_3}x_2^2\right)\exp\left(-\frac{j\pi}{\lambda f_2}x_2^2\right)\exp\left(\frac{-j2\pi_1}{\lambda d_2}x_2x_1\right)\exp\left(\frac{-j2\pi}{\lambda d_3}x_2x_3\right)\right]\\
&= \exp\left(\frac{j\pi}{\lambda d_3}x_3^2\right)\exp\left(\frac{j\pi}{\lambda d_1}x_0^2\right)A(x_0)\int_{-\infty}^{+\infty}\mathrm{d}x_1 P(x_1)\Phi(x_1)\exp\left[\frac{j\pi}{\lambda}\left(\frac{1}{d_1}+\frac{1}{d_2}-\frac{1}{f_1}\right)x_1^2\right]\exp\left(\frac{-j2\pi}{\lambda d_1}x_0x_1\right)\\
&\quad\times\left\{\int_{-\infty}^{+\infty}\mathrm{d}x_2\exp\left[\frac{j\pi}{\lambda}\left(\frac{1}{d_2}+\frac{1}{d_3}-\frac{1}{f_2}\right)x_2^2\right]\exp\left[\frac{-j2\pi}{\lambda}\left(\frac{x_1}{d_2}+\frac{x_3}{d_3}\right)x_2\right]\right\},
\end{aligned}
\tag{1}
$$

where a prefactor is dropped. $A(x_0)$ is the strength of the point source at x_0 of the sample plane, and λ is the wavelength of the illumination. To simplify Eq. (1), we define β and γ as

$$\beta = \frac{1}{\frac{1}{d_1}+\frac{1}{d_2}-\frac{1}{f_1}} \quad \text{and} \quad \gamma = \frac{1}{\frac{1}{d_2}+\frac{1}{d_3}-\frac{1}{f_2}}. \tag{2}$$

Then, Eq. (1) can be rewritten as

$$\begin{aligned} G(x_3,x_0) &= \exp\left(\frac{j\pi}{\lambda d_3}x_3^2\right)\exp\left(\frac{j\pi}{\lambda d_1}x_0^2\right)A(x_0) \\ &\times \int_{-\infty}^{+\infty} \mathrm{d}x_1 P(x_1)\Phi(x_1)\exp\left(\frac{j\pi}{\lambda\beta}x_1^2\right) \\ &\times \exp\left(\frac{-j2\pi}{\lambda d_1}x_0x_1\right) \\ &\times \left\{\int_{-\infty}^{+\infty}\mathrm{d}x_2\ \exp\left(\frac{j\pi}{\lambda\gamma}x_2^2\right)\right. \\ &\left.\times\exp\left[\frac{-j2\pi}{\lambda}\left(\frac{x_1}{d_2}+\frac{x_3}{d_3}\right)x_2\right]\right\} \\ &= \exp\left[\frac{j\pi}{\lambda}\left(\frac{1}{d_3}-\frac{\gamma}{d_3^2}\right)x_3^2\right]\exp\left(\frac{j\pi}{\lambda d_1}x_0^2\right)A(x_0) \\ &\times \int_{-\infty}^{+\infty}\mathrm{d}x_1 P(x_1)\Phi(x_1)\exp\left[\frac{j\pi}{\lambda}\left(\frac{1}{\beta}-\frac{\gamma}{d_2^2}\right)x_1^2\right] \\ &\times \exp\left[-j2\pi\left(\frac{\gamma x_3}{\lambda d_2 d_3}+\frac{x_0}{\lambda d_1}\right)x_1\right]. \end{aligned} \tag{3}$$

To further simplify Eq. (3), we define the general pupil function as

$$P_1(x_1) = P(x_1)\Phi(x_1)\Phi_d(x_1), \tag{4}$$

where

$$\Phi_d(x_1) = \exp\left[\frac{j\pi}{\lambda}\left(\frac{1}{\beta}-\frac{\gamma}{d_2^2}\right)x_1^2\right], \tag{5}$$

which is the defocus term of the system. The defocus term becomes unity if the CCD is at image plane of the sample. Now, Eq. (1) can be simplified as

$$\begin{aligned} G(x_3,x_0) &= \exp\left[\frac{j\pi}{\lambda}\left(\frac{1}{d_3}-\frac{\gamma}{d_3^2}\right)x_3^2\right] \\ &\times \exp\left(\frac{j\pi}{\lambda d_1}x_0^2\right)A(x_0)T\left(\frac{\gamma d_1}{d_2 d_3}x_3+x_0\right), \end{aligned} \tag{6}$$

where

$$T\left(\frac{\gamma d_1}{d_2 d_3}x_3+x_0\right) = FT\{P_1(x_1)\}|_{f_x=\frac{1}{\lambda d_1}\left(\frac{\gamma d_1}{d_2 d_3}x_3+x_0\right)}, \tag{7}$$

where FT denotes Fourier transform. The complex amplitude of the optical field of an extended object at the CCD plane is obtained by superposition of the amplitude PSF of all the source points, which is given by

$$\begin{aligned} O(x_3) &= \Phi_q(x_3)\int_{-\infty}^{+\infty}\mathrm{d}x_0 \\ &\times \exp\left[\frac{j\pi}{\lambda d_1}(x_0^2)\right]A(x_0)T\left(\frac{\gamma d_1}{d_2 d_3}x_3+x_0\right), \end{aligned} \tag{8}$$

where $\Phi_q(x_3)$ is given by

$$\Phi_q(x_3) = \exp\left[\frac{j\pi}{\lambda}\left(\frac{1}{d_3}-\frac{\gamma}{d_3^2}\right)x_3^2\right]. \tag{9}$$

This quadratic phase term appears outside the integrals in Eqs. (6) and (8). It plays a crucial role in the image correction, as will be validated in the following two sections. From the guide-star hologram, we can obtain the amplitude PSF given by Eq. (6). Removing $\Phi_q(x_3)$ from the amplitude PSF and setting the source point at origin, we can obtain a modified amplitude PSF, as follows:

$$G_1(x_3) = A_0 T\left(\frac{\gamma d_1}{d_2 d_3}x_3\right). \tag{10}$$

Similarly, a modified field of the extended object can be obtained from the full-field hologram and numerical removal of the quadratic phase term $\Phi_q(x_3)$, as follows:

$$O_1(x_3) = \int_{-\infty}^{+\infty}\mathrm{d}x_0\exp\left[\frac{j\pi}{\lambda d_1}(x_0^2)\right]A(x_0)T\left(\frac{\gamma d_1}{d_2 d_3}x_3+x_0\right). \tag{11}$$

Correlating this modified field with the modified amplitude PSF given by Eq. (10), we have

$$\begin{aligned} O_1 \otimes G_1(x_3) &= A_0\int_{-\infty}^{+\infty}\int_{-\infty}^{+\infty}\mathrm{d}\alpha\mathrm{d}x_0 \times \exp\left[\frac{j\pi}{\lambda d_1}(x_0^2)\right]A(x_0) \\ &\times T\left(\frac{\gamma d_1}{d_2 d_3}x_3+x_0+\frac{\gamma d_1}{d_2 d_3}\alpha\right)T^*\left(\frac{\gamma d_1}{d_2 d_3}\alpha\right) \\ &= \frac{d_2 d_3 A_0}{\gamma d_1}\int_{-\infty}^{+\infty}\int_{-\infty}^{+\infty}\mathrm{d}\alpha\mathrm{d}x_0 \\ &\times \exp\left[\frac{j\pi}{\lambda d_1}(x_0^2)\right]A(x_0) \\ &\times T\left(\frac{\gamma d_1}{d_2 d_3}x_3+x_0+\alpha\right)T^*(\alpha), \end{aligned} \tag{12}$$

where $\otimes$ denotes correlation. According to the definition in Eq. (7), we have

$$T\left(x_0+\frac{\gamma d_1}{d_2 d_3}x_3+\alpha\right)$$
$$=\int_{-\infty}^{+\infty}\mathrm{d}\eta P_1(\eta)\exp\left[\frac{-j2\pi}{\lambda d_1}\eta\left(x_0+\frac{\gamma d_1}{d_2 d_3}x_3+\alpha\right)\right] \quad (13)$$

and

$$T^*(\alpha)=\int_{-\infty}^{+\infty}\mathrm{d}x P_1^*(x)\exp\left(\frac{j2\pi}{\lambda d_1}\alpha x\right). \quad (14)$$

Plugging Eqs. (13) and (14) into Eq. (12), the correlation operation results in

$$\begin{aligned}FT\{G(x_3,0)\}&=A_0 FT\left\{\exp\left[\frac{j\pi}{\lambda}\left(\frac{1}{d_3}-\frac{\gamma}{d_3^2}\right)x_3^2\right]T\left(\frac{\gamma d_1}{d_2 d_3}x_3\right)\right\}\\&=A_0 FT\left\{\exp\left[\frac{j\pi}{\lambda}\left(\frac{1}{d_3}-\frac{\gamma}{d_3^2}\right)\left(\frac{\lambda d_2 d_3}{\gamma}\right)^2 f_x^2\right]\right\}\\&\quad\times\odot FT\{FT\{P_1(x_1)\}(f_x)\}\\&=\frac{A_0\gamma}{d_2\sqrt{-j\lambda(d_3-\gamma)}}\\&\quad\times\exp\left[\frac{-j\pi\gamma^2}{\lambda(d_3-\gamma)d_2^2}x_1^2\right]\odot P_1(-x_1), \quad (17)\end{aligned}$$

$$\begin{aligned}O_1\otimes G_1(x_3)&=\frac{d_2 d_3 A_0}{\gamma d_1}\int_{-\infty}^{+\infty}\int_{-\infty}^{+\infty}\mathrm{d}\alpha\mathrm{d}x_0\exp\left[\frac{j\pi}{\lambda d_1}(x_0^2)\right]A(x_0)\\&\quad\times\left\{\int_{-\infty}^{+\infty}\mathrm{d}\eta P_1(\eta)\exp\left[\frac{-j2\pi}{\lambda d_1}\eta\left(x_0+\frac{\gamma d_1}{d_2 d_3}x_3+\alpha\right)\right]\int_{-\infty}^{+\infty}\mathrm{d}x P_1^*(x)\exp\left(\frac{j2\pi}{\lambda d_1}\alpha x\right)\right\}\\&=\frac{d_2 d_3 A_0}{\gamma d_1}\int_{-\infty}^{+\infty}\mathrm{d}x_0\exp\left[\frac{j\pi}{\lambda d_1}(x_0^2)\right]A(x_0)\\&\quad\times\int_{-\infty}^{+\infty}\int_{-\infty}^{+\infty}\mathrm{d}x\mathrm{d}\eta P_1^*(x)P_1(\eta)\exp\left[\frac{-j2\pi}{\lambda d_1}\eta\left(x_0+\frac{\gamma d_1}{d_2 d_3}x_3\right)\right]\left\{\int_{-\infty}^{+\infty}\mathrm{d}\alpha\exp\left[\frac{j2\pi}{\lambda d_1}(x-\eta)\alpha\right]\right\}\\&=\frac{\lambda d_2 d_3 A_0}{\gamma}\int_{-\infty}^{+\infty}\mathrm{d}x_0\exp\left(\frac{j\pi}{\lambda d_1}x_0^2\right)A(x_0)\int_{-\infty}^{+\infty}\int_{-\infty}^{+\infty}\mathrm{d}x\mathrm{d}\eta P_1^*(x)P_1(\eta)\exp\left[\frac{-j2\pi}{\lambda d_1}\eta\left(x_0+\frac{\gamma d_1}{d_2 d_3}x_3\right)\right]\delta(x-\eta)\\&=\frac{\lambda d_2 d_3 A_0}{\gamma}\int_{-\infty}^{+\infty}\mathrm{d}x_0\exp\left(\frac{j\pi}{\lambda d_1}x_0^2\right)A(x_0)\int_{-\infty}^{+\infty}\mathrm{d}x P_1^*(x)P_1(x)\exp\left[\frac{-j2\pi}{\lambda d_1}x\left(x_0+\frac{\gamma d_1}{d_2 d_3}x_3\right)\right]\\&=\frac{\lambda d_2 d_3 A_0}{\gamma}\int_{-\infty}^{+\infty}\mathrm{d}x_0\exp\left(\frac{j\pi}{\lambda d_1}x_0^2\right)A(x_0)\int_{-\infty}^{+\infty}\mathrm{d}x P(x)\exp\left[\frac{-j2\pi}{\lambda d_1}x\left(x_0+\frac{\gamma d_1}{d_2 d_3}x_3\right)\right], \quad (15)\end{aligned}$$

From Eq. (15), the correlation operation removes both the aberration term $\Phi(x_1)$ and the defocus term $\Phi_d(x_1)$, obtaining a corrected and focused image no matter where the CCD is put. The magnification of this corrected image is given by $-(d_2 d_3)/\gamma d_1$. Although our derivation is based on a two-lens system, the conclusion thus rendered can be generalized to any optical system. The difference lies in the specific expressions for the defocus term $\Phi_d(x_1)$ and the global quadratic phase term $\Phi_q(x_3)$. According to the convolution theorem, Eq. (15) can be implemented by

$$O_1\otimes G_1(x_3)=IFT\{FT\{O_1(x_3)\}FT^*\{G_1(x_3)\}\}, \quad (16)$$

where IFT denotes the inverse Fourier transform. $O(x_3)$ and $G(x_3)$ can be obtained through off-axis holography [14–19]. Eliminating the quadratic phase term $\Phi_q(x_3)$ from $O(x_3)$ and $G(x_3)$, we can get $O_1(x_3)$ and $G_1(x_3)$. To achieve the fields $O_1(x_3)$ and $G_1(x_3)$ correctly, the sampling requirements have to be taken into account. Taking FT of the amplitude PSF of the source point at origin, we have

where $\odot$ denotes the convolution operation and f_x is the spatial frequency in the horizontal direction,

$$f_x=\frac{\gamma}{\lambda d_2 d_3}x_3. \quad (18)$$

Expanding Eq. (17), it becomes the spectrum of a finite chirp function. The width of this spectrum can estimated as that of the general pupil function [17,27,28]. Because the sampling requirement for the one-dimensional case is different from that for the two-dimensional case, let us now consider the two-dimensional case. If the CCD has $M\times N$ square pixels with side length Δx_3, then the sampling spacings of the spatial frequency along the horizontal and vertical dimensions are given by

$$\Delta f_x=\Delta f_y=\frac{\gamma}{\lambda d_2 d_3}\Delta x_3. \quad (19)$$

Then the sampling spacings on two dimensions at the pupil plane are given by [18,19]

$$\Delta x_1 = \frac{\lambda d_2 d_3}{N\gamma\Delta x_3} \quad \text{and} \quad \Delta y_1 = \frac{\lambda d_2 d_3}{M\gamma\Delta x_3}. \tag{20}$$

Assume the diameter of a round pupil is D that is estimated as the width of the image order of the hologram, and the width of zero-order of the hologram is twice that of the image order. To recover the optical field at the pupil plane, the pupil size D has to satisfy [29]

$$D \le \frac{\sqrt{2}\lambda d_2 d_3}{4\gamma\Delta x_3}. \tag{21}$$

Finally, it is worth mentioning that a special case of the correlation method is FTDHAO, where d_2 and d_3 are equal to f_2 [20]. Then Eq. (21) evolves into the expression for the sampling requirement in FTDHAO.

3. Simulations

In the simulations, the focal lengths, f_1 and f_2, of the lens L1 and L2 are set to be 25 and 200 mm, respectively. We set d_1, the distance between the sample and the lens L1, to be 25 mm. The group 4 elements 2–5 of USAF1951 resolution target are used to simulate the amplitude of the sample, as shown by Fig. 2(a). The field of view is 780 μm × 780 μm. The pixel pitch is 3.9 μm. A random phase noise ranging from $-\pi$ to π simulates the phase distribution of the sample, as illustrated by Fig. 2(b). All the phase profiles throughout this paper are displayed in blue-white-red color map that corresponds to $[-\pi, \pi]$. The wavelength of the laser beam is set to be 0.633 μm. We present three simulation samples, corresponding to three different combinations of d_2 and d_3. In the first case, d_2 is set to be 200 mm and d_3 to be 150 mm. Then γ is calculated as 150 mm, according to Eq. (2), and Φ_q becomes unity. The CCD is put at a defocus plane of the sample. The defocus term Φ_d is given by Eq. (5). The simulation results are presented in Fig. 2. Figure 2(c) is the undistorted but defocused field at the CCD plane when no aberration is added at the pupil plane. The sampling spacing of the spatial frequency in either direction is 0.031 line pairs/mm. For the purpose of comparison, we propagate it to the image plane. The undistorted focused image is shown in Fig. 2(d). Figure 2(e) shows the simulated phase aberration Φ added at the pupil plane, which is given by two sixth-order Zernike polynomials $4\pi(Z_6^2 + Z_6^4) = 4\pi(15r^6 - 20r^4 + 6r^2)[\cos(2\theta) + \sin(2\theta)]$. From the full-field hologram, we can retrieve the field at the CCD plane that is distorted by this added phase aberration Φ, as shown in Fig. 2(f). Propagating this distorted field to the focal plane, we can obtain the focused but degraded image, as shown by Fig. 2(g). Taking FT of the distorted field shown by Fig. 2(f) results in the

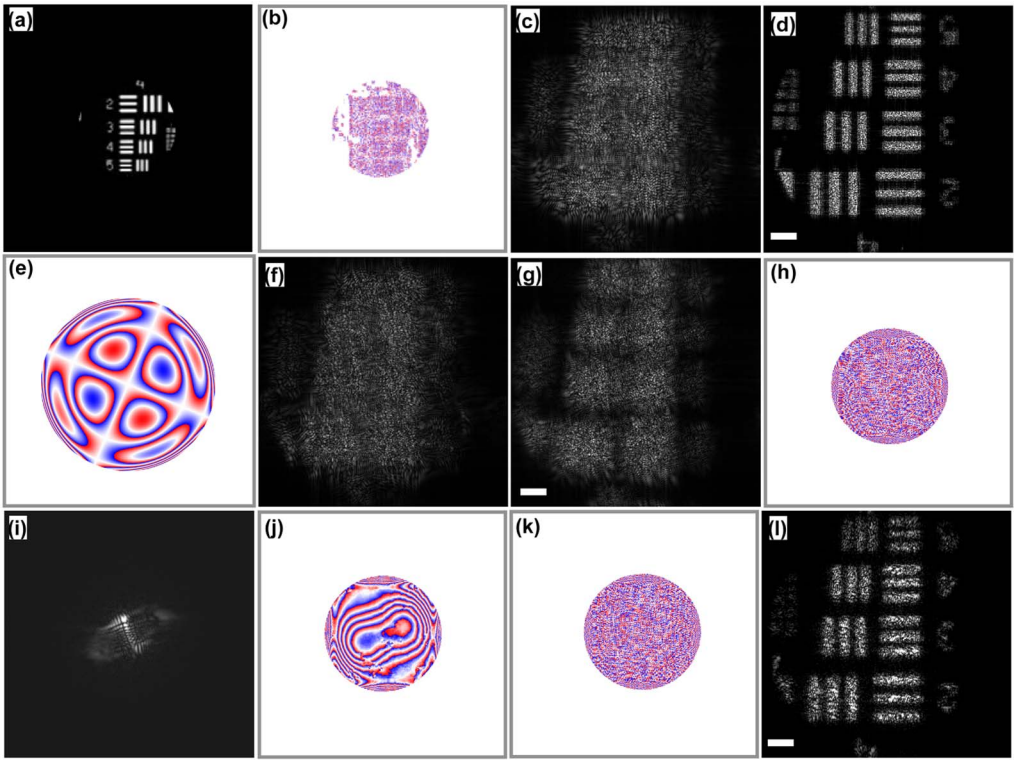

Fig. 2. Simulation example where the defocus term Φ_d exists and the global quadratic phase term Φ_q is unity. (a),(b) Simulated amplitude and phase. The phase maps are represented by blue-white-red color map that corresponds to $[-\pi, \pi]$. (c) Optical field at the CCD plane without aberrator in place. (d) Focused image of (c). (e) Simulated phase aberration Φ. (f) Full-field aberrated hologram at the CCD plane. (g) Focused image of (f). (h) Full-field phase profile at the pupil with aberration. (i) Guide-star hologram, i.e., the amplitude PSF of the system. (j) General pupil function that is the FT of (i). (k) Corrected field at the pupil. (l) Corrected image from (k).

distorted field at the pupil, which contains both the added aberration Φ and the defocus term Φ_d, as shown in Fig. 2(h). The spatial sampling spacing of this distorted field is 21 μm. From the guide-star hologram, the amplitude PSF of the system is obtained, which is shown in Fig. 2(i). The general pupil function that is the FT of the amplitude PSF is shown in Fig. 2(j). The root mean square (RMS) measurement error of the phase of the general pupil function is 0.97 rad that corresponding to about 0.15 wavelengths. Subtracting Fig. 2(j) from Fig. 2(h), we can get the corrected field at the pupil, which is given by Fig. 2(k). As described by Eq. (16), the corrected image can be obtained by taking IFT of Fig. 2(k), which is shown in Fig. 2(l). Compared to the defocused and distorted field in Fig. 2(f), the correlation operation eliminates the aberration and meanwhile automatically focuses the corrected field.

In the second case, d_2 is set to be 300 mm and d_3 to be 200 mm. The defocus term Φ_d becomes unity, which signifies the CCD is at the image plane of the sample. However, in this scheme, the global quadratic phase term Φ_q is not unity, which is given by Eq. (9). The simulation results are shown in Fig. 3. The baseline image, without aberration in place, is shown in Fig. 3(a). Figure 3(b) shows the image distorted by the aberration Φ illustrated in Fig. 2(e). Figure 3(c) shows the affected field at the pupil. The amplitude PSF of this system is shown in Fig. 3(d). The measured aberration at the pupil is given by Fig. 3(e). The RMS measurement error of the phase of the general pupil function is 0.91 rad that corresponding to about 0.14 wavelengths. Figure 3(f) illustrates the corrected image that shows remarkable improvement in resolution and quality, compared to the distorted image in Fig. 3(b). In this case, removal of the quadratic phase term Φ_q before the correlation operation is found to be of significance in the correction. The effect of this term on the corrected image is shown in Fig. 4. Figure 4(a) shows the measured aberration at the pupil when Φ_q is not eliminated before the correlation operation, and Fig. 4(c) illustrates the corresponding corrected image, which is much degraded compared to Fig. 3(f), that is obtained with Φ_q removed. If Φ_q is partially removed, the recovered image becomes better, compared to that with Φ_q untreated. Figure 4(b) shows the measured aberration at the pupil when Φ_q is

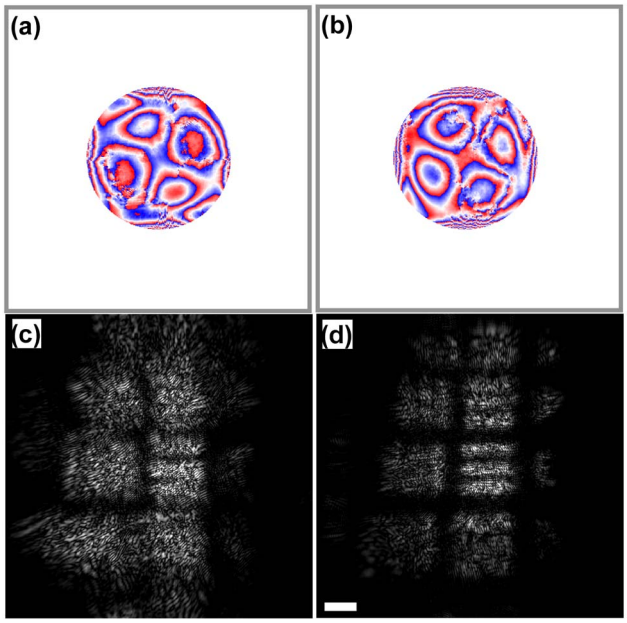

Fig. 4. Demonstration of the effect of Φ_q on the corrected image. (a) Measured aberration at the pupil when Φ_q is not eliminated. (b) Measured aberration at the pupil when Φ_q is partially eliminated. (c) Image corrected by (a). (d) Image corrected by (b).

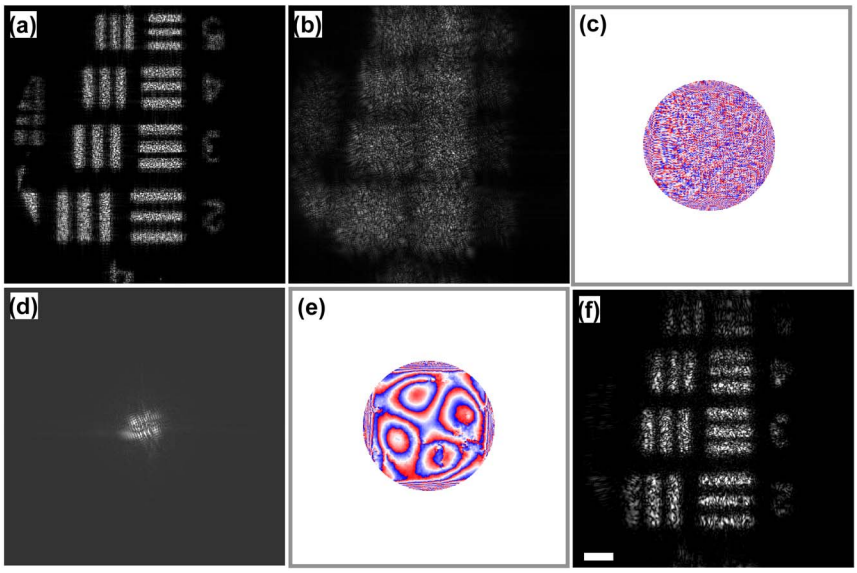

Fig. 3. Simulation example where Φ_q exists while Φ_d is unity. (a) Undistorted optical field at CCD plane. (b) Distorted field at the CCD plane. (c) Distorted field at the pupil. (d) Amplitude PSF of the system. (e) General pupil function. (f) Corrected image.

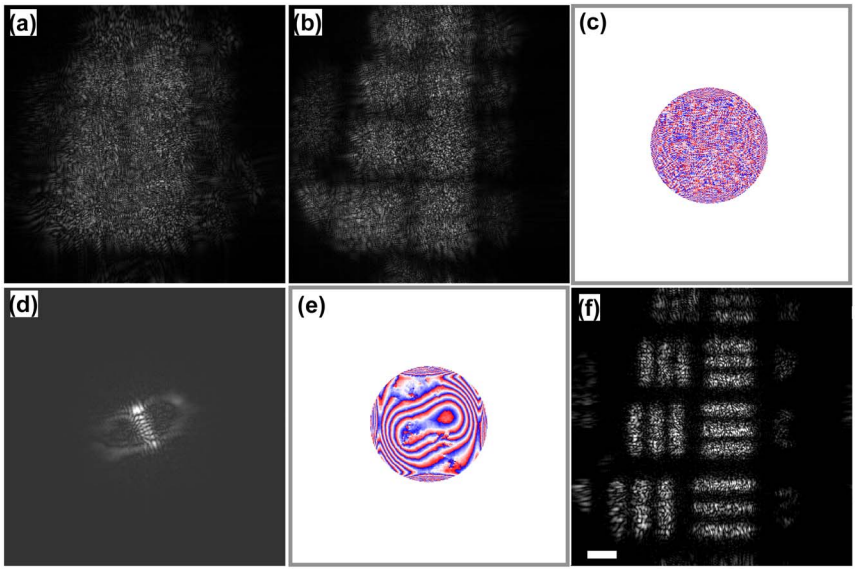

Fig. 5. Simulation example where both Φ_q and Φ_d exist. (a) Distorted optical field at the CCD plane. (b) Distorted image. (c) Distorted field at the pupil. (d) Amplitude PSF of the system. (e) General pupil function. (f) Corrected image.

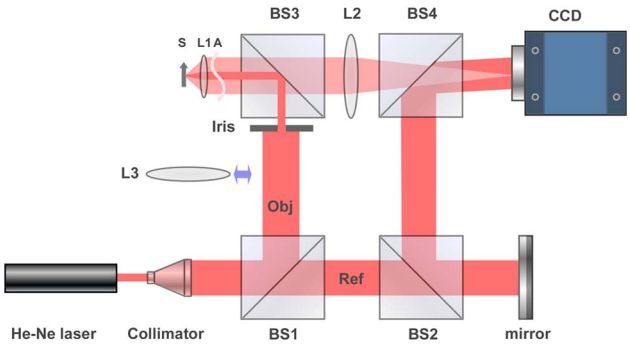

Fig. 6. Schematic diagram of the experimental apparatus. S, sample; L1–L3, lens; A, aberrator; BS1-4, beam splitters.

partially eliminated, and Fig. 4(d) shows the corresponding corrected image.

The third simulation sample demonstrates a general case where both Φ_q and Φ_d exist. In this case, we set d_2 to be 300 mm and d_3 to be 150 mm. The simulation results are shown in Fig. 5. Figure 5(a) shows the distorted full field at the CCD plane that is defocused and distorted. Note that the quadratic phase term Φ_q has been eliminated. The focused but distorted image is shown in Fig. 5(b). The distorted field at the pupil is given by Fig. 5(c), which includes the added aberration Φ and defocus term Φ_d. The amplitude PSF of this system is shown in Fig. 5(d). Again, the quadratic phase term Φ_q has been eliminated.

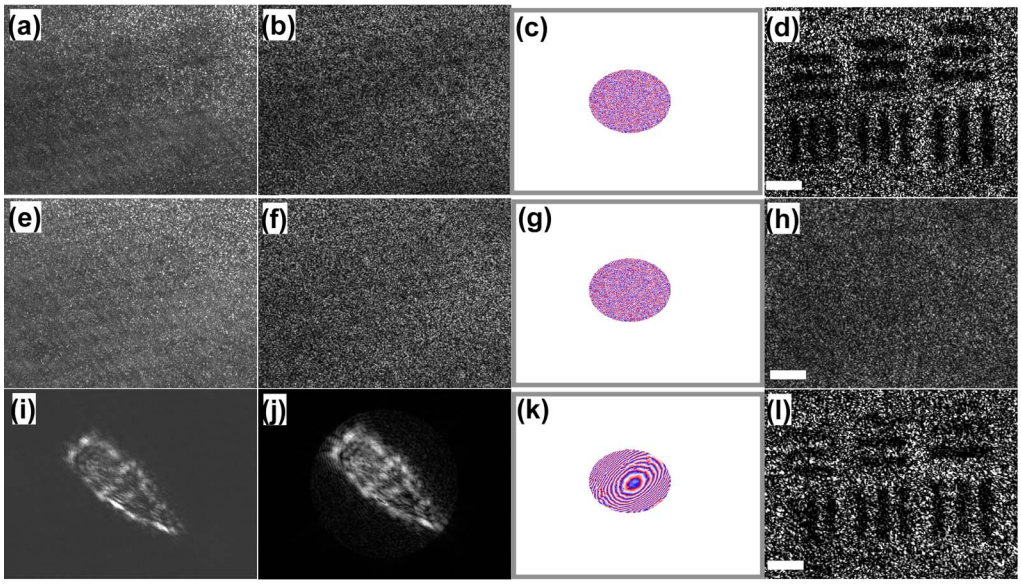

Fig. 7. Experimental example where the defocus term Φ_d exists while the global quadratic phase term Φ_q is unity. (a) Hologram without aberration. (b) Amplitude at the CCD plane. (c) Undistorted field at the pupil. (d) Undistorted image. (e) Distorted hologram. (f) Distorted field at the CCD plane. (g) Distorted field at the pupil. (h) Distorted image. (i) Guide-star hologram. (j) Amplitude PSF of the system. (k) General pupil function. (l) Corrected image.

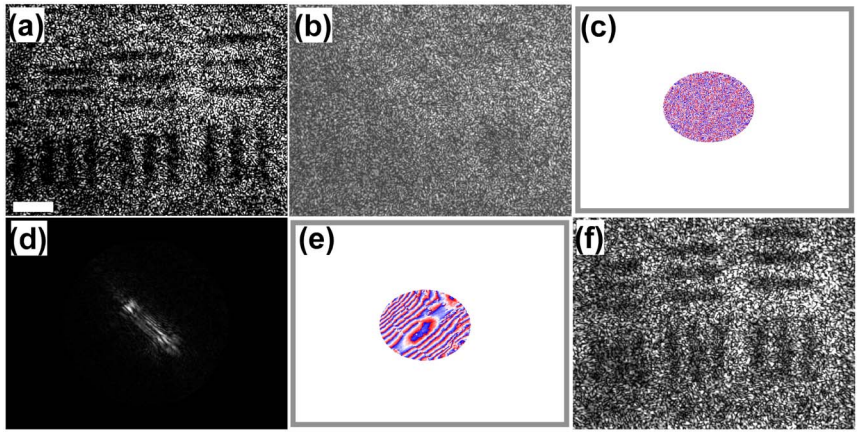

Fig. 8. Experimental example where Φ_q exists while Φ_d takes unity. (a) Undistorted image. (b) Distorted image. (c) Distorted full field at the pupil. (d) Amplitude PSF of the system. (e) Measured aberration. (f) Corrected image.

The FT of this amplitude PSF is given by Fig. 5(e) that includes Φ and Φ_d. The RMS measurement error of the phase map represented by Fig. 5(e) is 0.88 rad that corresponding to about 0.14 wavelengths. Removing Fig. 5(e) from Fig. 5(c) and taking IFT, we can get the corrected image shown in Fig. 5(f). The resolution is completely recovered and the defocus is eliminated.

4. Experimental Results and Discussions

The schematic diagram of the experimental setup is illustrated in Fig. 6. The focal length f_1 of the lens L1 is 25 mm. S represents the sample plane that is at the back focal plane of eye lens E. Hence, d_1 equals 25 mm. The phase aberrator A is close to the pupil of the lens L1. The focal length f_2 of L2 is 200 mm. The CCD has 1024×768 pixels with the pixel pitch 6.45 μm. In our experiments, He–Ne laser is used as light source. The sample under test is a positive USAF 1951 resolution target with a piece of Teflon tape tightly attached behind. The specular reflection is blocked by the pupil whose size is set to be 5 mm in diameter, and the CCD receives the diffuse scattered light from the Teflon tape. A piece of clear broken glass serves as the phase aberrator. The Lens L3 is inserted for full-field illumination. Corresponding to the three simulation cases, we present three experimental examples by choosing different values of d_2 and d_3. In the first example, we set d_2 to be 200 mm and d_3 to be 150 mm, which indicates the CCD is at a defocus plane of the sample. The defocus term Φ_d is calculated by Eq. (5). According to Eq. (9), the quadratic phase term Φ_q becomes unity. A set of image data is shown in Fig. 7. The field of view on the sample plane is 594 μm × 445 μm. The full-field hologram, without the aberrator in place, is shown in Fig. 7(a). By the holographic process, the complex optical field at the CCD plane can be achieved, which is shown in Fig. 7(b) [15–19]. The sampling spacing of the spatial frequency at the CCD plane is 0.037 line pairs/mm in either direction, according to Eq. (19). Taking FT of this field, the full optical field at the pupil is obtained, as shown in Fig. 7(c). According to Eq. (20), the spatial sampling spacings along the horizontal and vertical directions are 27 and 35 μm, respectively. For the purpose of comparison, we propagate this defocused field at the CCD plane illustrated by Fig. 7(b) to the image plane, and obtain the undistorted focused image shown in Fig. 7(d), serving as a baseline. The distorted full-field hologram is shown in Fig. 7(e), from which we can get the distorted and defocused field at the CCD plane, as shown in Fig. 7(f). The distorted full field at the pupil is shown in Fig. 7(g), which contains the added aberration and the defocus term. Figure 7(h) is the distorted image. The guide-star hologram is shown in Fig. 7(i), from which we obtain the amplitude PSF of the system that is illustrated by Fig. 7(j). Figure 7(k) shows the general pupil function. Subtracting Fig. 7(k) from Fig. 7(g), we get the corrected

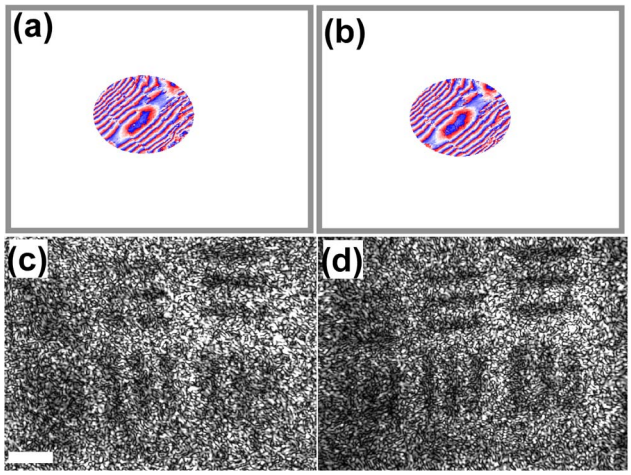

Fig. 9. Experimental demonstration of the effect of Φ_q on the corrected image. (a) Measured aberration at the pupil when Φ_q is not eliminated. (b) Measured aberration at the pupil when Φ_q is partially eliminated. (c) Image corrected by (a). (d) Image corrected by (b).

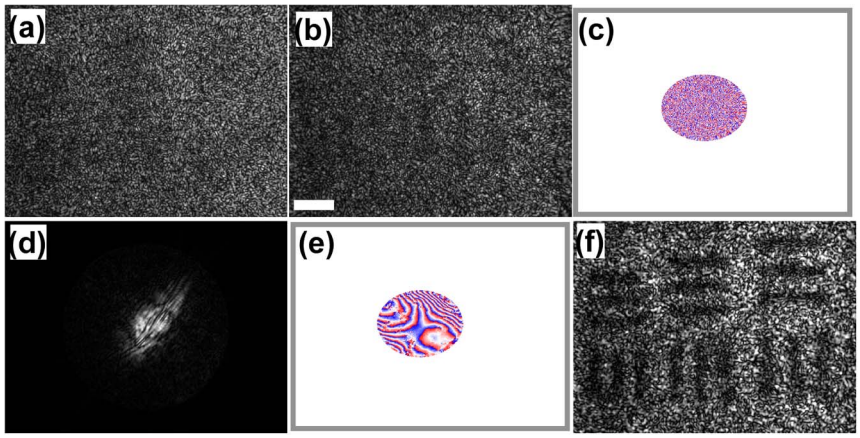

Fig. 10. Experimental example where both Φ_q and Φ_d exist. (a) Distorted optical field at CCD plane. (b) Distorted image. (c) Distorted field at the pupil. (d) Amplitude PSF of the system. (e) Phase map of the FT of (d). (f) Corrected image.

field at the pupil. As described by Eq. (16), the corrected image can be obtained by taking IFT of this corrected field, which is shown in Fig. 7(l). Compared to the defocused and distorted field in Fig. 7(f), the correlation operation eliminates both the aberration and the defocus term.

In the second example, we set d_2 to be 150 mm and d_3 to be 200 mm, which indicates the CCD is at the image plane of the sample. The defocus term Φ_d disappears while the quadratic phase term Φ_q exists. Figure 8(a) shows the baseline image. The distorted image is illustrated by Fig. 8(b). Figure 8(c) shows the distorted full field at the pupil. The amplitude PSF of the system is illustrated by Fig. 8(d). Figure 8(e) is the measured aberration at the pupil. The recovered image is shown in Fig. 8(f). The resolution and contrast are almost completely recovered. Note that the quadratic phase term Φ_q has to be removed before the correlation operation. The effect of this term on the corrected image is also demonstrated in this example, shown in Fig. 9. Figure 9(a) shows the measured aberration at the pupil when Φ_q is not eliminated before the correlation operation, and Fig. 9(c) shows corresponding corrected image, which is rather blurred compared to Fig. 8(f). When Φ_q is partially removed, the recovered image becomes better. Figure 9(b) shows the measured aberration at the pupil when Φ_q is partially eliminated and Fig. 9(d) shows the corresponding corrected image.

For the third experimental sample, d_2 is 150 mm and d_3 250 mm. This is a general case where both Φ_q and Φ_d exist. The results are shown in Fig. 10. Figure 10(a) shows the distorted field at the CCD plane that is defocused and distorted. Note that the quadratic phase term Φ_q has been eliminated. The focused but distorted image is shown in Fig. 10(b). The distorted full field at the pupil is given by Fig. 10(c). The amplitude PSF of this system is illustrated by Fig. 10(d). Its FT is shown in Fig. 10(e). Subtracting Fig. 10(e) from Fig. 10(c) and taking IFT, we can get the corrected image that is shown in Fig. 10(f). The resolution is completely recovered and the defocus is eliminated.

5. Conclusions

In summary, a novel correction method is proposed for the DHAO system. It is realized through the correlation between the complex full-field hologram and complex guide-star hologram. By this method, both the aberration at the pupil and the defocus of the system can be removed, which means it is not necessary to further propagate the corrected full field to the image plane, wherever the CCD is. It is worth noting that if the global phase term Φ_q does exist, it has to be removed before the correlation operation. Otherwise, the aberrations cannot be correctly compensated for. Although our derivation is based on a two-lens system, the conclusion can be generalized to any optical system, if the optical aberrations of the system mainly lie at or close to the pupil plane. It generalizes the FTDHAO into arbitrary DHAO systems and provides us a guidance to design new experimental schemes for applications in AO in ophthalmology and microscopy. The measurement error of the phase aberration is due mainly to the deviation of the guide-star spot from the ideal point source. The size of the incident beam at the pupil in the first passage for the guide-star hologram is usually set to be about 2 mm in diameter to minimize the effect of the aberration and generate a sharp guide star. From simulations and experiments, this error does exist but is not severe. Also, coherent noise seems inevitable if laser is used as the light source. This can be addressed by use of low coherent light source [21,22,25].

Research reported in this paper was supported by the National Eye Institute of the National Institutes of Health under Award No. R21EY021876. The content is solely the responsibility of the authors and does not necessarily represent the official views of the National Institutes of Health.

References

1. H. W. Babcock, "The possibility of compensating astronomical seeing," Publ. Astron. Soc. Pac. **65**, 229–236 (1953).
2. M. A. van Dam, D. Le Mignant, and B. A. Macintosh, "Performance of the Keck observatory adaptive optics system," Appl. Opt. **43**, 5458–5467 (2004).
3. M. Hart, "Recent advances in astronomical adaptive optics," Appl. Opt. **49**, D17–D29 (2010).
4. J. Liang, B. Grimm, S. Goelz, and J. Bille, "Objective measurement of wave aberrations of the human eye with the use of a Hartmann-Shack wave-front sensor," J. Opt. Soc. Am. A **11**, 1949–1957 (1994).
5. J. Liang, D. R. Williams, and D. Miller, "Supernormal vision and high-resolution retinal imaging through adaptive optics," J. Opt. Soc. Am. A **14**, 2884–2892 (1997).
6. A. Roorda, F. Romero-Borja, W. J. Donnelly III, H. Queener, T. J. Herbert, and M. C. W. Campbell, "Adaptive optics scanning laser ophthalmoscopy," Opt. Express **10**, 405–412 (2002).
7. K. M. Hampson, "Adaptive optics and vision," J. Mod. Opt. **55**, 3425–3467 (2008).
8. I. Iglesias, R. Ragazzoni, Y. Julien, and P. Artal, "Extended source pyramid wave-front sensor for the human eye," Opt. Express **10**, 419–428 (2002).
9. N. Doble, G. Yoon, L. Chen, P. Bierden, B. Singer, S. Olivier, and D. R. Williams, "Use of a microelectromechanical mirror for adaptive optics in the human eye," Opt. Lett. **27**, 1537–1539 (2002).
10. S. R. Chamot, C. Dainty, and S. Esposito, "Adaptive optics for ophthalmic applications using a pyramid wavefront sensor," Opt. Express **14**, 518–526 (2006).
11. Q. Mu, Z. Cao, D. Li, and L. Xuan, "Liquid crystal based adaptive optics system to compensate both low and high order aberrations in a model eye," Opt. Express **15**, 1946–1953 (2007).
12. M. J. Booth, D. Debarre, and A. Jesacher, "Adaptive optics for biomedical microscopy," Opt. Photonics News **23**, 22–29 (2012).
13. M. J. Booth, "Adaptive optics in microscopy," Phil. Trans. R. Soc. A **365**, 2829–2843 (2007).
14. C. Liu and M. K. Kim, "Digital holographic adaptive optics for ocular imaging: proof of principle," Opt. Lett. **36**, 2710–2712 (2011).
15. U. Schnars and W. Jüptner, "Direct recording of holograms by a CCD target and numerical reconstruction," Appl. Opt. **33**, 179–181 (1994).
16. E. Cuche, P. Marquet, and C. Depeursinge, "Digital holography for quantitative phase-contrast imaging," Opt. Lett. **24**, 291–293 (1999).
17. C. Liu, D. Wang, and Y. Zhang, "Comparison and verification of numerical reconstruction methods in digital holography," Opt. Eng. **48**, 1058021 (2009).
18. M. K. Kim, "Principles and techniques of digital holographic microscopy," SPIE Rev. **1**, 018005 (2010).
19. M. K. Kim, *Digital Holographic Microscopy: Principles, Techniques, and Applications* (Springer, 2011), pp. 55–93.
20. C. Liu, X. Yu, and M. K. Kim, "Fourier transform digital holographic adaptive optics imaging system," Appl. Opt. **51**, 8449–8454 (2012).
21. F. Dubois, L. Joannes, and J. C. Legros, "Improved three-dimensional imaging with digital holography microscope with a source of partial spatial coherence," Appl. Opt. **38**, 7085–7094 (1999).
22. G. Pedrini and H. J. Tiziani, "Short-coherence digital microscopy by use of lensless holographic imaging system," Appl. Opt. **41**, 4489–4496 (2002).
23. M. K. Kim, "Adaptive optics by incoherent digital holography," Opt. Lett. **37**, 2694–2696 (2012).
24. M. K. Kim, "Incoherent digital holographic adaptive optics," Appl. Opt. **52**, A117–A130 (2013).
25. F. Dubois and C. Yourassowsky, "Full off-axis red-green-blue digital holographic microscope with LED illumination," Opt. Lett. **37**, 2190–2192 (2012).
26. R. Kelner and J. Rosen, "Spatially incoherent single channel digital Fourier holography," Opt. Lett. **37**, 3723–3725 (2012).
27. J. Goodman, *Introduction to Fourier Optics*, 3rd ed. (Roberts & Company, 2005), pp. 105–107.
28. L. Onural, "Some mathematical properties of the uniformly sampled quadratic phase function and associated issues in digital Fresnel diffraction simulation," Opt. Eng. **43**, 2557–2563 (2004).
29. N. Pavillon, C. S. Seelamantula, J. Kühn, M. Unser, and C. Depeursinge, "Suppression of the zero-order term in off-axis digital holography through nonlinear filtering," Appl. Opt. **48**, H186–H195 (2009).